Supporting Information

Bercovici et al. 10.1073/pnas.1205004109

SI Text

SI Materials and Methods. ***Numerical model of isotachophoresis-based hybridization.*** Here, we show details of our novel kinetics model to capture the hybridization reaction of two nucleic acid species under isotachophoresis (ITP) conditions. Defining A, B as single-stranded nucleic acid species and AB as double stranded hybrid, the reaction equation is expressed as

$$\mathrm{A} + \mathrm{B} \underset{k_{\mathrm{off}}}{\overset{k_{\mathrm{on}}}{\rightleftarrows}} \mathrm{AB}, \qquad \text{[S1]}$$

where k_{on} and k_{off} are respectively the reaction on- and off-rate constants. ITP drives simultaneous mixing and focusing of reactants into a common electromigrating reaction zone in which reaction is accelerated due to the high concentration of reactants. For simplicity, we consider a case in which the species A and B are initially mixed with LE and TE, respectively (in practice, we can alternately mix together both species in TE and/or LE, allowing reaction to start as soon as reagents are mixed). This process is qualitatively described in Fig. 1.

Assuming negligible electroosmotic flow, we can neglect radial electromigration and radial diffusion associated with advective dispersion, so that the concentration distribution and electric field vary only along the axial coordinate of the channel (1, 2). The area-averaged, coupled electromigration-diffusion-reaction conservation equations for species A, B, and AB can then be expressed as

$$\begin{aligned}
&\text{(i)}\ \frac{\partial c_{\mathrm{A}}}{\partial t} + \frac{\partial}{\partial x}\left[(\mu_{\mathrm{A}}E - V_{\mathrm{ITP}})c_{\mathrm{A}} - D_{\mathrm{A}}\frac{\partial c_{\mathrm{A}}}{\partial x}\right] = -k_{\mathrm{on}}c_{\mathrm{A}}c_{\mathrm{B}} + k_{\mathrm{off}}c_{\mathrm{AB}}\\
&\text{(ii)}\ \frac{\partial c_{\mathrm{B}}}{\partial t} + \frac{\partial}{\partial x}\left[(\mu_{\mathrm{B}}E - V_{\mathrm{ITP}})c_{\mathrm{B}} - D_{\mathrm{B}}\frac{\partial c_{\mathrm{B}}}{\partial x}\right] = -k_{\mathrm{on}}c_{\mathrm{A}}c_{\mathrm{B}} + k_{\mathrm{off}}c_{\mathrm{AB}}\\
&\text{(iii)}\ \frac{\partial c_{\mathrm{AB}}}{\partial t} + \frac{\partial}{\partial x}\left[(\mu_{\mathrm{AB}}E - V_{\mathrm{ITP}})c_{\mathrm{AB}} - D_{\mathrm{AB}}\frac{\partial c_{\mathrm{AB}}}{\partial x}\right]\\
&\quad = k_{\mathrm{on}}c_{\mathrm{A}}c_{\mathrm{B}} - k_{\mathrm{off}}c_{\mathrm{AB}}, \qquad \text{[S2]}
\end{aligned}$$

where μ_i and D_i respectively denote electrophoretic mobility and diffusivity of each species; i represents species A, B, or AB; and E is the local electric field. We define the electrophoretic mobility as $\mu = u/E$ where u is species drift velocity.

Under the negligible electroosmotic flow assumption, V_{ITP} can be expressed as $\mu_{\mathrm{LE}}j/\sigma_{\mathrm{LE}}$ where j is the current density along the microchannel and σ_{LE} is the conductivity of the LE buffer. We assume that ITP is controlled by constant applied current in which the velocity of ITP interface, V_{ITP}, remains approximately constant. The width of the ITP interface is determined by a balance between diffusion and electromigration, and following MacInnes and Longsworth (3), it takes the form of

$$\delta_{\mathrm{theory}} = \frac{RT}{FV_{\mathrm{ITP}}}\left(\frac{\mu_{\mathrm{LE}}\mu_{\mathrm{TE}}}{\mu_{\mathrm{LE}} - \mu_{\mathrm{TE}}}\right), \qquad \text{[S3]}$$

where R is the universal gas constant, T is the temperature, and F is Faraday's constant (1–3). Subscripts "TE" and "LE" denote respectively properties of the TE and LE anions. Under ideal conditions and constant applied current, ITP theory predicts peak mode ITP will maintain constant interface width over time. However, in practice several factors may cause an increase in the interface width (e.g., time varying residual electroosmotic flow) (4, 5). Thus, we assume the ITP interface width to be a function of time, $\delta(t)$, to sustain general applicability of the model. As shown in Fig. 1 we define a control volume moving at a constant interface velocity V_{ITP} and extending over a distance, L, which is significantly larger than the ITP interface width, δ, at all times.

We integrate Eq. **S2** over this control volume (per unit area of channel). Assuming diffusive fluxes are zero at the control volume boundaries, the electromigration and diffusive flux terms (the second term on the lefthand side) become known area integrals at the inlet and outlet. For the source terms involving species concentrations, the contribution of the integral outside the interface width is negligible since the species concentrations are several orders of magnitude greater within the interface than beyond the interface. Thus, we approximate the integrals of concentration over the control volume size, L, by the integrals over a region very near the interface width, δ:

$$\int_L c_i dx \approx \int_\delta c_i dx. \qquad \text{[S4]}$$

We then define average concentrations, $\bar{c}_i$ as

$$\bar{c}_i = \frac{1}{\delta}\int_\delta c_i dx. \qquad \text{[S5]}$$

In treating the volume-averaged source terms $\bar{c}_{\mathrm{A}}\bar{c}_{\mathrm{B}}$ and $\bar{c}_{\mathrm{AB}}$, we assume that concentration distributions of species A, B, and AB are Gaussian in shape, and that all of these Gaussian peaks are located at the same axial coordinate within the ITP interface. This assumption is considered as reasonable when the mobilities of analytes are significantly greater and significantly less than those of TE and LE, respectively, and when analyte concentrations are significantly lower than those of the TE and LE, as we consider here (2). This enables us to approximate the concentration profile of each species as

$$c_i = c_i^{\max} e^{-\frac{x^2}{2\sigma^2}} \quad \text{for } i = \mathrm{A}, \mathrm{B}, \quad \text{and} \quad \mathrm{AB}, \qquad \text{[S6]}$$

where σ is the standard deviation of the Gaussian profile of the species (all σ are assumed equal). Given this assumption, we elaborate on the control-volume-integration over the interface width from the Eq. **S4** as equal to an integral over -3σ to $+3\sigma$ of the Gaussian concentration profiles. Thus, the integration across the interface width covers approximately 99.7% of the area under each c_i profile. Using these integration limits, the mixed term $\bar{c}_{\mathrm{A}}\bar{c}_{\mathrm{B}}$, which appears in the integration of Eq. **S2**, can be approximated as

$$\bar{c}_{\mathrm{A}}\bar{c}_{\mathrm{B}} = \frac{3}{\sqrt{\pi}}\bar{c}_{\mathrm{A}}\bar{c}_{\mathrm{B}}. \qquad \text{[S7]}$$

Again, the integration boundaries reflect the fact that hybridization product is produced only within the narrow ITP interface region, while influx of species (and their contribution to global accumulation rates) can be estimated relatively far from the interface. Combining the assumptions and approximations given above, we derive control-volume-averaged equations as:

$$\text{(i)}\ \frac{d\bar{c}_A}{dt} = \frac{\eta_{TE} V_{ITP}}{\delta} A_0 - \frac{1}{\delta}\frac{d\delta}{dt}\bar{c}_A - \frac{3}{\sqrt{\pi}} k_{on}\bar{c}_A\bar{c}_B + k_{off}\bar{c}_{AB}$$

$$\text{(ii)}\ \frac{d\bar{c}_B}{dt} = \frac{\eta_{LE} V_{ITP}}{\delta} B_0 - \frac{1}{\delta}\frac{d\delta}{dt}\bar{c}_B - \frac{3}{\sqrt{\pi}} k_{on}\bar{c}_A\bar{c}_B + k_{off}\bar{c}_{AB} \quad \textbf{[S8]}$$

$$\text{(iii)}\ \frac{d\bar{c}_{AB}}{dt} = -\frac{1}{\delta}\frac{d\delta}{dt}\bar{c}_{AB} + \frac{3}{\sqrt{\pi}} k_{on}\bar{c}_A\bar{c}_B - k_{off}\bar{c}_{AB},$$

where η_{TE} and η_{LE} are

$$\eta_{TE} = \left[\left(\frac{\mu_A}{\mu_{TE}} - 1\right)\frac{\mu_{TE}}{\mu_{LE}}\frac{\mu_{CI} - \mu_{LE}}{\mu_{CI} - \mu_{TE}}\frac{c_{LE}}{c_{TE}^{well}}\right] \quad \text{and} \quad \eta_{LE} = 1 - \frac{\mu_B}{\mu_{LE}}. \quad \textbf{[S9]}$$

Here, subscript CI denotes the (cationic) counter ion. The superscript "*well*" denotes an upstream reservoir property. A_0 and B_0 represent the reservoir concentrations of species A and B respectively in the TE and LE. We solve this set of non-linear ordinary differential equations (ODE) numerically to describe the simultaneous focusing and reaction dynamics of the volume averaged species concentrations over time.

Analytical model of ITP-based hybridization. Starting from the numerical model shown in Eq. **S8**, we derive an analytical solution by making two key assumptions. The first, most restrictive assumption states that the ITP interface width remains constant over time, $\delta(t) = \delta_o$, such that the terms involving derivative of δ can be eliminated. In this limit, the time integrals of linear combinations of Eq. **S8** yield simpler equations for the conservation of species relations:

$$\text{(i)}\ \bar{c}_A + \bar{c}_{AB} = \frac{\eta_{TE} V_{ITP}}{\delta_o} A_0 t \qquad \text{(ii)}\ \bar{c}_B + \bar{c}_{AB} = \frac{\eta_{LE} V_{ITP}}{\delta_o} B_0 t. \quad \textbf{[S10]}$$

Here, the grouping $\eta_{TE} V_{ITP}/\delta_o$ is the ITP focusing coefficient of species A in units of inverse time, so $\eta_{TE} V_{ITP} A_0 t/\delta_o$ is the total concentration of species A at the ITP interface. We use this conservation of species relations to express $\bar{c}_A$ and $\bar{c}_B$ in terms of $\bar{c}_{AB}$. Before continuing, we highlight a key difference between the standard second-order reaction kinetics and ITP-based hybridization kinetics. As ITP continuously focuses reactants into the interface, the total concentrations of species A and B continuously and linearly increase over time. This results in an increase in the available reactant concentrations within the interface. The conservation relations are therefore in sharp contrast to those of the standard second-order reaction kinetics, (namely, $c_A + c_{AB} = A_0$ and $c_B + c_{AB} = B_0$) wherein total concentrations are fixed at the initial values.

We further impose conditions on initial reservoir concentrations of A and B, namely A_0 and B_0. We assume that one species has excess concentration at the ITP interface, and that the equilibrium constant is sufficiently low. These can be expressed as:

$$\eta_{TE} A_0 \gg \eta_{LE} B_0 \quad \text{and} \quad \frac{\eta_{TE} V_{ITP}}{\delta_o} A_0 t \gg K. \quad \textbf{[S11]}$$

These conditions are in fact less restrictive than the standard model's assumptions of $A_0 \gg B_0$ and $k_{off}/k_{on} \ll A_0$, since the value of η_{TE} is typically several times larger than η_{LE}, and the ITP focusing coefficient $\eta_{TE} V_{ITP}/\delta_o$ is typically order 10. Substituting Eq. **S10** and applying these assumptions to Eq. **S8**, iii, the latter simplifies to the following linear, inhomogeneous ODE with non-constant coefficients:

$$\frac{d\bar{c}_{AB}}{dt} + 2at\bar{c}_{AB} = bt^2, \quad \textbf{[S12]}$$

where

$$a = \frac{3}{\sqrt{\pi}}\frac{k_{on}}{2}\frac{\eta_{TE} V_{ITP}}{\delta_o} A_0 \quad \text{and}$$

$$b = \frac{3}{\sqrt{\pi}} k_{on}\eta_{TE}\eta_{LE}\left(\frac{V_{ITP}}{\delta_o}\right)^2 A_0 B_0.$$

This equation can be readily solved using variation of parameters. After applying the initial condition of $\bar{c}_{AB} = 0$ at $t = 0$, the analytical solution to the differential equation is obtained as

$$\bar{c}_{AB} = \frac{b}{2a}\left[t - \frac{1}{2}\sqrt{\frac{\pi}{a}} e^{-at^2} erfi(\sqrt{at})\right], \quad \textbf{[S13]}$$

where *erfi* is the imaginary error function, $erfi(x) = -ierf(ix)$ (which yields real quantities). We refer to this solution throughout the paper as the exact analytical solution of ITP hybridization kinetics. Expanding *erfi* in a Taylor series and keeping only the leading order term yields the approximate analytical solution:

$$\bar{c}_{AB} \cong \underbrace{\frac{\eta_{LE} V_{ITP}}{\delta_o} B_0 t}_{B_{0,ITP}}\left(1 - e^{-\frac{3}{2\sqrt{\pi}}\frac{\eta_{TE} V_{ITP}}{\delta_o} A_0 k_{on} t^2}\right). \quad \textbf{[S14]}$$

Effects of current density and measurement position on reaction kinetics. We use the approximate analytical model to further analyze the effects of current density, j, and measurement position, x, on the reaction kinetics and fraction of completion of ITP dynamics. To explore its physical meaning, we scale Eq. **S14**, with the steadily increasing term, $B_{0,ITP}$, and obtain the fraction of reactants hybridized:

$$f_{ITP} = \frac{\overline{c_{AB}}}{B_{0,ITP}} \cong 1 - \exp\left(-\frac{3}{2\sqrt{\pi}}\frac{\eta_{TE} V_{ITP}}{\delta_o} k_{on} A_0 t^2\right). \quad \textbf{[S15]}$$

The characteristic hybridization time scale for half of the reactants to be hybridized at the ITP interface is then given by

$$\tau_{ITP} \cong \sqrt{\frac{\ln 2}{\frac{\eta_{TE} V_{ITP}}{\delta_o} k_{on} A_0}}. \quad \textbf{[S16]}$$

We expand t, V_{ITP} and δ_o respectively using $t = x/V_{ITP}$, $V_{ITP} = \mu_{LE} j/\sigma_{LE}$ and $\delta_o = \delta_{theory}$ where δ_{theory} is the MacInnes and Longsworth's expression for the ITP interface width under peak mode ITP (Eq. **S3**). The fraction of reactants hybridized and the characteristic time scale in terms of x and j are given as

$$f_{ITP} \cong 1 - \exp\left(-\frac{3}{2\sqrt{\pi}}\frac{F}{RT}\frac{\eta_{TE}(\mu_{LE} - \mu_{TE})}{\mu_{LE}\mu_{TE}} k_{on} A_0 x^2\right), \quad \textbf{[S17]}$$

$$\tau_{ITP} \cong \frac{\sqrt{\ln 2}}{j\sqrt{\frac{F}{RT}\frac{\eta_{TE}\mu_{LE}(\mu_{LE} - \mu_{TE})}{\mu_{TE}\sigma_{LE}^2} k_{on} A_0}} \propto \frac{1}{j\sqrt{k_{on} A_0}}, \quad \textbf{[S18]}$$

where the symbol $\propto$ denotes proportionality. These forms highlight proportionalities important in designing ITP-based reaction experiments. For example, given values of k_{on} and A_0, the fraction of hybrid product in ITP is determined solely by the electromigration length and is approximately independent of the current density. Effectively, we can control the percentage of reactants

hybridized by changing the observation point in the microchannel. In the application of diagnostics or sequence detection, the higher percentage of reactants hybridized usually yields the brighter fluorescence intensity.

On the other hand, the characteristic reaction time is inversely proportional to ITP velocity and, therefore, to current density. For molecular-diffusion-limited dispersion, higher current yields thinner ITP zones and higher concentrations (2). This increases reaction rate, but also advects the reaction vessel downstream at a proportionally higher rate. Therefore, for a fixed observation location, higher current yields, to first order, faster reactions by decreasing time to travel the fixed distance. In practice, applied current is typically limited by either the maximum output voltage of the current source meter or by Joule heating considerations. Note the TE zone is most typically lower conductivity than the LE zone, so that required voltage increases as ITP progresses under galvanostatic conditions.

Comparison of the fraction of reactants hybridized for ITP versus standard hybridization. Here, we present comparison of ITP hybridization kinetics and standard second-order kinetics in terms of fraction of reactants hybridized. In the main article, we examined the figure of merit defined as τ_{std}/τ_{ITP} comparing the time scales of the ITP and standard reaction case. We explored the effect of varying reactant concentrations and kinetic on-rate constants. Here we define another figure of merit, the ratio of the expected hybrid fraction resulting from ITP to the hybrid fraction from the standard case, f_{ITP}/f_{std}. Fig. S1 uses the analytical model (Eq. **S14**) to calculate f_{ITP}/f_{std} as a function of time for variable $k_{on} \cdot A_0$ values. These curves show how ITP offers vastly higher reaction completion fractions at finite, relevant times. For example, at 200 s, the ITP-based hybridization at 100 pM with k_{on} of 10^3 M^{-1} s^{-1} ($k_{on} \cdot A_0$ of order 10^{-7} s^{-1}) shows roughly 5,000-fold higher fraction of reactants hybridized than standard case. As discussed in the next section, the increased hybrid concentrations translate to increased signal-to-noise ratio for experiments involving fluorescent hybrid products. Note B_0 does not appear in Fig. S1 since the results of the analytical model are not a function of B_0 under the assumption of $A_0 \gg B_0$.

Measurements of fraction of reactants hybridized. For experimental validation of our ITP-based kinetics model, we explored the hybridization kinetics of DNA molecular beacons (MBs) (6, 7) and synthetic DNA oligonucleotides (targets). In all experiments, we used DNA targets as species A and MBs as species B. Molecular beacons are fluorescent probes, which give typical signal enhancements of 10- to 100-fold upon hybridization to a target sequence (6, 8). MBs consist of a central probe sequence connected to two complementary stem sequences. A fluorophore is bound to the 5′ terminus of the MB, and a quencher to the 3′ terminus. In the absence of target, the stem sequences hybridize, forming a hairpin structure where the quencher inhibits fluorescence. In the presence of target, the MB stem preferentially unzips and the probe sequence binds to the target, separating the fluorophore from quencher to increase fluorescence signal.

In the absence of target, MBs exhibit residual background fluorescence due to the limited efficiency of the quencher and conformational fluctuation in equilibrium between closed and open (yet unhybridized) MBs (9). The MB's spontaneous-opening rate is significantly low compared to closing rate, thus we ignore the open (but unhybridized) state of MBs, and consider only the two states of MBs in this study: closed-MBs and hybrids. The two conformations of MB yield different levels of fluorescence signal. We use proportionality constants, α and β, to relate fluorescence level and concentration for the hybrids and closed MBs, respectively. The MB fluorescence signal when hybridized to a target, I_{AB}, can be normalized by the background fluorescence of MBs in the absence of target, I_B, to yield a signal-to-noise ratio, $SNR = I_{AB}/I_B$, associated with the sequence-specific MB-target hybridization. We express the relation between the SNR and the species concentrations as $SNR = (\alpha c_{AB} + \beta c_B)/\beta B_0$ (B_0 is replaced by $B_{0,ITP}$ for ITP cases). We can rearrange this equation to express the fraction of reactants hybridized in terms of SNR:

$$f = \frac{SNR - 1}{\alpha/\beta - 1}. \quad \textbf{[S19]}$$

We use this as the relation to convert experimentally measurable quantity (SNR) into a predictable quantify, f.

For standard second-order kinetics, as the reaction is taken to completion ($c_B \to 0$ and $c_{AB} \to B_0$), SNR approaches α/β, while f approaches unity. We can therefore measure α/β by estimating the steady state SNR value. We experimentally quantified α/β as 29.3 (±4.8STD) for standard hybridization and 36.3 (±2.3STD) for ITP hybridization. We obtained the former value using SNR data of the case in Fig. 4. For the latter value, we used the ensemble average and standard deviation (STD) of SNR at steady state from the experiments shown in Fig. S2. We hypothesize that the difference between the two cases is associated with the fact that MBs under ITP are in an inhomogeneous buffer field (e.g., roughly half resides in LE, and half in TE). Different buffering agents and slight pH differences between TE (pH = 7.3) and LE (pH = 6.5) may, for example, change fluorescence yield. When analyzing experimental data, we used corresponding α/β values for each case.

Microchannel preparation. For all hybridization experiments, we used single, straight channels fabricated from free-standing capillaries. This setup let us achieve a cheap and reusable microchannel with a suitably small inner diameter to minimize the effects of dispersion on ITP preconcentration (2). We glued 21 μm inner diameter, 360 μm outer diameter, and 40 mm (50 mm for the demonstration experiment in Fig. 4) long circular capillaries (TPS020375, Polymicro Technologies) on a 2.5 cm × 7.5 cm glass cover slide (micro slides, VWR). We burned away the polyimide coating using a lighter. We used the ∼1 cm long larger end of 1–200 μL pipette tips (VWR) as reservoirs. We glued the capillary and the two reservoirs on the glass slide using UV-cure optical adhesive (Optical Adhesive 68, Norland Products Inc.), and cured the glue under a portable UV lamp (B-100A, IVP) for 15 min. Once the glue hardened, we covered the entire length of the capillary with the same optical adhesive glue to match the index of refraction, and then cured under a UV lamp for another 40 min for complete cure. Prior to each set of experiments, we cleaned the microchannel by flowing 200 mM NaOH for 2 min, and then rinsed it with DI water for 2 min.

Experimental measurement of parameters. Kinetic on-rate constant measurement. We conducted independent standard hybridization experiments using premixed reactants solution for quantitation of k_{on}. We dissolved molecular beacons (species B) at a concentration of 10 nM and targets (species A) at concentrations of 2.5, 5, and 10 μM in a buffer identical to the LE buffer used in ITP hybridization experiments. These concentrations satisfy the assumption of one species present in excess concentration, thus we use the standard second-order reaction solution,

$$f_{std} = c_{AB}/B_0 = 1 - e^{-k_{on}A_0 t}, \quad \textbf{[S20]}$$

to extract the on-rate constant. We used an external vacuum source to flow the mixture of A and B into a microchannel, and used the detection system of Fig. 2*A* to quantify beacon fluorescence signals versus time. We continued recording the fluores-

cence signal until there was little change in fluorescence intensity over time (indicating steady state of reaction).

To analyze the data we first subtract the buffer-only background signal from the raw fluorescence intensity versus time data. We then divide this background-subtracted signal by the MB background in the absence of target (fluorescence intensity before adding target) to obtain the SNR. We convert SNR to fraction of reactants hybridized, $f_{std} = c_{AB}/B_0$, using Eq. **S19**. In Fig. S2*A*, we present a plot of f_{std} versus $A_0 t$ for the experimental data (symbols) and a nonlinear regression fit (solid line). As per Eq. **S20**, all data collapsed into a single curve on a time axis normalized by $1/A_0$, which confirms that the time scale of this reaction is proportional to the inverse of concentration of excess species. We estimate the value of k_{on} as 4750 $M^{-1} s^{-1}$ using a nonlinear least squares fit on all data points, and report the 95% confidence interval of ± 2 $M^{-1} s^{-1}$ for the fitting parameter, k_{on}. We employed the "fit" function of MATLAB, which is based on the trust-region-reflective algorithm (10). For all theory predictions, we substitute this measured parameter value of k_{on} in the model.

Fig. S2*B* shows the fraction of reactants hybridized, f_{std}, versus time on a log basis for the same data. Here, we also include an additional experimental result using 10 and 20 nM concentrations of MB and target DNA, respectively. The solid lines indicate the theory predictions based on Eq. **S20** using the experimentally measured value of k_{on}. The comparison between theory and experimental data shows how a single value of k_{on} predicts observable hybridization reaction kinetics across a wide range of reactant concentrations. Note the case of 10 nM MB and 20 nM target hybridization (diamonds) falls just outside the applicability of the model, and yet the model fairly well captures the associated slow kinetics.

Experimental measurements of ITP parameters. We measured ITP velocity, V_{ITP} and ITP interface width, δ from the ITP hybridization experiments, and used those values for the required parameters in model solutions. As shown in Fig. 5*B* of the main article, the raw data recorded from ITP-based hybridization experiment consists of seven peaks in approximate Gaussian shape. We fit each peak with a Gaussians distribution in the form of $I = Ae^{(t-\mu)^2/2\sigma^2}$ where I is the fluorescence intensity, A is the amplitude, μ is the mean, and σ is the standard deviation of the Gaussian peak. The example raw data, Gaussian fit and all relevant parameters are shown in Fig. S3. We define the ITP interface width δ as 6σ of each peak.

In Fig. S4*A*, we present the peak position versus time data and its linear regression fit. We used the slope of the fit, 107 μm/s, as the value of V_{ITP} throughout the paper. We observed interface width increased with time as shown in Fig. S4*B*. For the numerical solutions, we approximated $\delta(t)$ as a first order polynomial: $\delta(t) = mt + b$, extracted the slope, m, and y-intercept, b, using a linear regression fit. For the analytical model, we assumed for simplicity a time-invariant interface width,δ_o , and used the time averaged and ensemble averaged values of δ resulting in a value of 59 μm.

These data also provide a measure of the repeatability of the time of arrival and interface width data. We calculated coefficient of variations at each observation location. The maximum values of coefficient of variation were 4.9 % and 11.7%, respectively, for the data shown in Fig. S4 *A* and *B*. Previous studies (11, 12) have shown that ITP-aided nucleic acid hybridization is robust and repeatable. Refs. 11 and 12 each present repeats of the ITP-based hybridization data as well as application to very different targets: Persat et al. 11 for detection of micro-RNA sequences from total RNA samples of various tissues, and Bercovici et al. 12 for *Escherichia coli* 16S rRNA from urine samples. For example, the study by Bercovici et al. 12 includes an overlay of 37 repeats of current versus time data for ITP-aided hybridization, and these have a coefficient of variation of less than 3%.

The parameter values used in the numerical and analytical model predictions can be summarized as follows: V_{ITP} is 107 μm/s, k_{on} is 4750 $M^{-1} s^{-1}$, the slope and y-intercept of $\delta(t)$ are 0.4 μm/s and 12.7 μm, respectively, δ_o is 59 μm, $\eta_{TE} = 7.8$ and $\eta_{LE} = 0.48$ using DNA mobility of 3.8×10^8 $m^2 V^{-1} s^{-1}$ [an estimate based on Stellwagen 13] for our 39-mer MBs and targets.

Comparison of analytical and numerical model. We developed the analytical model based on two key assumptions: excess of one species over the other at the reaction region formed by the ITP interface, $\gamma = \eta_{TE} A_0 / \eta_{LE} B_0 \gg 1$, and a constant interface width. Here we evaluate the effect of each assumption on the accuracy of the solution, by comparing three different models:

1. *Numerical model 1* assumes co-located Gaussian shape concentration profiles of all focused species, constant ITP velocity, and a linearly increasing ITP interface width, $\delta(t) = mt + b$. This model is obtained by numerically integrating Eq. **S8**. We used experimentally measured parameter values, $V_{ITP} = 107$ μm/s, $\delta(t) = mt + b$, with measured values of 0.4 μm/s and 12.7 μm for m and b, respectively, and our measured value of $k_{on} = 4750$ $M^{-1} s^{-1}$ (see *SI* Experimental measurement of parameters). This model was used in Fig. 3 as the numerical model lines.
2. *Numerical model 2* shares all the assumptions of numerical model 1, but also assumes a constant ITP interface width, $\delta(t) = \delta_o$. The assumption of constant interface width simplifies Eq. **S8** into Eq. **S15**, but these must still be solved numerically. We used an ensemble averaged and time averaged ITP interface width value of 59 μm. This model is not presented in Fig. 3, but plotted in Fig. S5. The equations describing this model are simply,

$$\begin{aligned} &\text{(i)}\ \frac{d\bar{c}_A}{dt} = \frac{\eta_{TE} V_{ITP}}{\delta_o} A_0 - \frac{3}{\sqrt{\pi}} k_{on} \bar{c}_A \bar{c}_B + k_{off} \bar{c}_{AB} \\ &\text{(ii)}\ \frac{d\bar{c}_B}{dt} = \frac{\eta_{LE} V_{ITP}}{\delta_o} B_0 - \frac{3}{\sqrt{\pi}} k_{on} \bar{c}_A \bar{c}_B + k_{off} \bar{c}_{AB} \\ &\text{(iii)}\ \frac{d\bar{c}_{AB}}{dt} = \frac{3}{\sqrt{\pi}} k_{on} \bar{c}_A \bar{c}_B - k_{off} \bar{c}_{AB}. \end{aligned} \qquad \textbf{[S21]}$$

3. *The exact analytical model* assumes both constant ITP interface width and excess of one species over the other. This model is described by Eq. **S13**, and is used for the analytical prediction lines shown in Fig. 3.

Fig. S5 presents a comparison of all three models. Each calculation is based on the same parameters as in Fig. 3. First, we focus on the cases with $\gamma = 16$ and 160 values, which satisfy the assumption of one excess species. Cleary, the assumption of a constant interface width (made by numerical model 2 and the analytical model) results in some deviation from the varying delta model (numerical model 1). This effect of constant width is particularly important at short times where hybridization rate is under-predicted by the analytical model. It is less important at long times and the analytical model only slightly overpredicts the expected values. Importantly, for this regime of γ values, we see that there are only negligible differences between model 2 and the analytical model. This suggests that the additional assumption of one excess species in the regime of $\gamma = 10$ or greater results in negligible error. Second, we comment on the case of $\gamma = 1.6$. As discussed, the constant width assumption resulted in under- then over-prediction error of the analytical model at respectively short and intermediate times. However, in addition to this, we see for the $\gamma = 1.6$ case that the overprediction by the analytical model is

more severe at long times. In summary, we conclude that most of the error in the analytical model relative to the numerical model can be attributed to the simplifying constant width assumption. Also, we see that errors associated with violating the one excess concentration assumption are significant for γ values of order 1.6 or less, as expected.

1. Saville DA, Palusinski OA (1986) Theory of electrophoretic separations. Part I: Formulation of a mathematical model. *AIChE J* 32:207–214.
2. Garcia-Schwarz G, Bercovici M, Marshall LA, Santiago JG (2011) Sample dispersion in isotachophoresis. *J Fluid Mech* 679:455–475.
3. MacInnes D, Longsworth L (1932) Transference numbers by the method of moving boundaries. *Chem Rev* 11:171–230.
4. Khurana TK, Santiago JG (2008) Sample zone dynamics in peak mode isotachophoresis. *Anal Chem* 80:6300–6307.
5. Khurana TK, Santiago JG (2009) Effects of carbon dioxide on peak mode isotachophoresis: Simultaneous preconcentration and separation. *Lab Chip* 9:1377–1384.
6. Tyagi S, Kramer FR (1996) Molecular beacons: Probes that fluoresce upon hybridization. *Nat Biotechnol* 14:303–308.
7. Bonnet G, Tyagi S, Libchaber A, Kramer FR (1999) Thermodynamic basis of the enhanced specificity of structured DNA probes. *Proc Natl Acad Sci USA* 96:6171–6176.
8. Kuhn H, et al. (2002) Hybridization of DNA and PNA molecular beacons to single-stranded and double-stranded DNA targets. *J Am Chem Soc* 124:1097–1103.
9. Bonnet G, Krichevsky O, Libchaber A (1998) Kinetics of conformational fluctuations in DNA hairpin-loops. *Proc Natl Acad Sci USA* 95:8602–8606.
10. Coleman TF, Li Y (1996) An interior trust region approach for nonlinear minimization subject to bounds. *SIAM J Optim* 6:418–445.
11. Persat A, Santiago JG (2011) MicroRNA profiling by simultaneous selective isotachophoresis and hybridization with molecular beacons. *Anal Chem* 83:2310–2316.
12. Bercovici M, et al. (2011) Rapid detection of urinary tract infections using isotachophoresis and molecular beacons. *Anal Chem* 83:4110–4117.
13. Stellwagen NC, Gelfi C, Righetti PG (1997) The free solution mobility of DNA. *Biopolymers* 42:687–703.

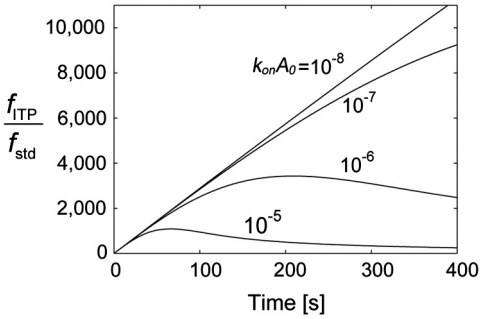

Fig. S1. Ratio of fractions of reactants hybridized for the ITP-based hybridization and standard hybridization as a function of time. The curves are plotted using the analytical model for ITP hybridization kinetics. For long times, the values approach unity since f_{std} and f_{ITP} each approach unity. f_{ITP}/f_{std} values greater than unity imply that f_{ITP} reaches the state of complete hybridization (in ITP zone) faster than f_{std}. The parameter values used for calculations are $\eta_{TE} = 50$, $V_{ITP} = 100$ μm/s, and $\delta_o = 50$ μm (same as Fig. 2 of the main article).

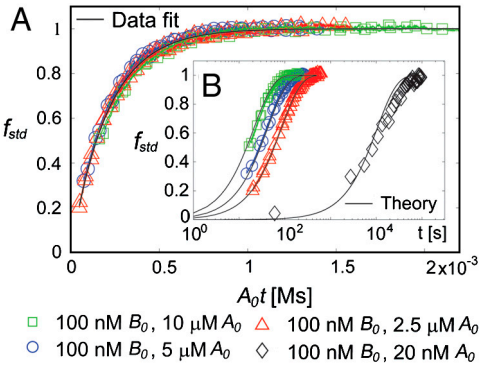

Fig. S2. Measurements of the molecular beacon kinetic on-rate constant, k_{on}. We explored the kinetic behavior of the MBs at 21 °C using a set of fluorescence measurements over time at a range of MB and target DNA concentrations. The data were taken with a sampling rate of 66.7 Hz, and the various symbols represent different target and MB concentrations, as indicated in the legend. (*A*) Experimental data for on-rate constant measurement (symbols) and nonlinear least square fit (solid line) are shown on a time axis weighted by A_0. We performed two repetitions for each target concentration. As per Eq. **S20**, all the fraction of reactants hybridized data, f_{std}, versus A_0t collapse into a single curve. We used a nonlinear least squares fit and obtained a k_{on} value of 4750 $M^{-1}s^{-1}$. We used this single, extracted k_{on} value in all of our model-based predictions. (*B*) Inset plot shows the same hybridization data and an additional measurements at a lower concentration, 10 nM MB and 20 nM target DNA, versus physical time. These are presented together with theory predictions (solid lines) based on the measured value of k_{on}. The latter data demonstrate that the use of our k_{on} value in the standard second order hybridization solution [Eq. **S20**] predicts hybridization kinetics for a wide range of concentrations. This includes the diamonds symbol series, which is a regime just outside the expected range of the model.

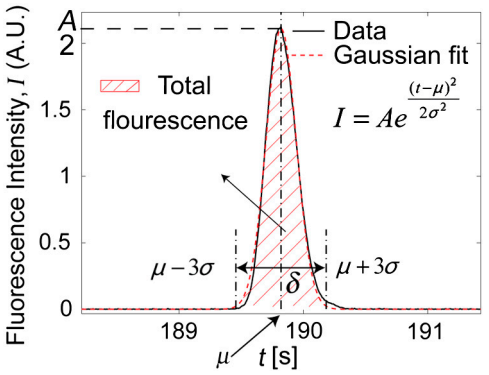

Fig. S3. Example raw ITP-based hybridization data (at one location) and its Gaussian fit. We first define the peak value as *A*, and the corresponding time as μ, and fit the data to a Gaussian distribution. We use the obtained standard deviation of the Gaussian fit to extract ITP interface width, defined as $\delta = 6\sigma$. We integrate the fluorescence intensity data ranging from $\mu - 3\sigma$ to $\mu + 3\sigma$, and obtain total fluorescence signal.

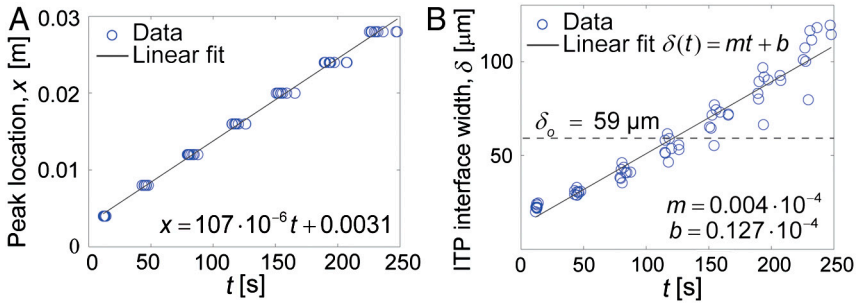

Fig. S4. Measurements of ITP interface velocity and width from experimental data. (*A*) The axial locations of the ITP peaks versus arrival times at each location, for the same ITP hybridization experiments shown in Fig. 3. $x = 0$ corresponds to the tip of the channel in the TE well, where ITP forms. Nine data points are shown at each peak location corresponding to three realizations at three target concentrations. We applied a linear regression fit (black solid line), and extracted an ITP velocity of 107 μm/s from the slope of the fit. (*B*) The measured ITP interface widths versus time (circles). We used a linear regression fit (solid black line) to obtain the slope and intercept values for the first order polynomial approximation of $\delta(t) = mt + b$. The average of all data points yielded the time and ensemble averaged value of ITP interface width, $\delta_o = 59$ μm, which we used for the analytical model.

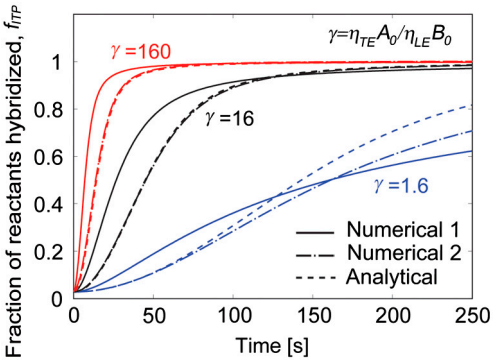

Fig. S5. Comparison of the analytical and numerical models for ITP-based hybridization kinetics. Shown are fractions of reactants hybridized $f_{ITP} = c_{BT,ITP}/B_{0,ITP}$ versus time at target concentrations of 1, 10, and 100 nM, and at a fixed molecular beacons concentration of 10 nM. Solid lines present numerical model 1 based on the coupled ordinary differential equations [Eq. **S8**] using a time-varying width function approximated as a first order polynomial. Dash-dot lines present numerical model 2 based on Eq. **S21** using the time-averaged constant ITP width. Dashed lines present the analytical model based on Eq. **S13**. Differences between the solid and dash-dot lines help demonstrate the errors associated with assuming a constant interface width, and the differences between the dash-dot and dashed lines demonstrate errors associated with violating the assumption that one species is in strong excess.